



21, rue d'Artois, F-75008 PARIS

<http://www.cigre.org>

## CIGRE US National Committee 2023 Grid of the Future Symposium

### **Powering the Future: Harnessing Neural Dynamic Equivalence for Enhanced Power System Applications**

**Q. SHEN<sup>1</sup>, Y. ZHOU<sup>1</sup>, H. ZHAO<sup>1</sup>, P. ZHANG<sup>1</sup>, Q. Zhang<sup>2</sup>, S. Maslennikov<sup>2</sup>, X. Luo<sup>2</sup>**

**1. Stony Brook University**

**2. ISO New England**

#### **SUMMARY**

Traditional grid analytics are model-based, relying strongly on accurate models of power systems, especially the dynamic models of generators, controllers, loads and other dynamic components. However, acquiring thorough power system models can be impractical in real operation due to inaccessible system parameters and privacy of consumers, which necessitate data-driven dynamic equivalencing of unknown subsystems. Learning reliable dynamic equivalent models for the external systems from SCADA and PMU data, however, is a long-standing intractable problem in power system analysis due to complicated nonlinearity and unforeseeable dynamic modes of power systems.

This paper advances a practical application of neural dynamic equivalence (NeuDyE) called Driving Port NeuDyE (DP-NeuDyE), which exploits physics-informed machine learning and neural-ordinary-differential-equations (ODE-NET) to discover a dynamic equivalence of external power grids while preserving its dynamic behaviors after disturbances with only boundary measurements. The new contributions are threefold:

- A NeuDyE formulation to enable a continuous-time, data-driven dynamic equivalence of power systems, saving the effort and expense of acquiring inaccessible system;
- An introduction of a Physics-Informed NeuDyE learning (PI-NeuDyE) to actively control the closed-loop accuracy of NeuDyE; and
- A DP-NeuDyE to reduce the number of inputs required for the training.

We conduct extensive case studies on the NPCC system to validate the generalizability and accuracy of both PI-NeuDyE and DP-NeuDyE. These exhaustive analyses span a multitude of scenarios, differing in the time required for fault clearance, the specific fault locations, and the limitations imposed by the accessibility of only a small subset of data. Test results have demonstrated the scalability and practicality of NeuDyE, showing its potential to be used in ISO and utility control centers for online transient stability analysis and for planning purposes.

#### **KEYWORDS**

Neural dynamic equivalence, ODE-NET, physics-informed machine learning, model order reduction, driving port.

Qing.shen@stonybrook.edu

## 1. INTRODUCTION

Reliable discovery of dynamic equivalent models for unidentified subsystems, specifically external systems, is crucial to ensure reliable operations of large-scale interconnected transmission systems [1]. However, this task has been a longstanding challenge due to the existence of nonlinear dynamics, complex coherency characteristics, and unavailable component models in power systems [2][3]. Recent advancements in Phasor Measurement Units (PMUs) provide an opportunity to readily obtain rich history of high-data-rate measurements, which fostered the development of data-driven dynamic equivalence [4]. Despite various attempts being reported in the literature, significant challenges persist:

- Learning continuous-time dynamic behaviors using discrete-time measurements poses a considerable obstacle. Traditional discretization techniques may not fully capture the intricacies of the continuous dynamics, leading to large inaccuracies that limit its practical implementations.
- Achieving robust and stable closed-loop operations under diverse operating conditions and disturbances is essential for safe plug-and-play integration of dynamic equivalence. Whereas, none of the existing dynamic equivalencing methods have achieved successful closed-loop operations with bulk power grid models.
- The final challenge lies in minimizing the required measurements to ensure a feasible and practical implementation.

This research makes three significant contributions to address the aforementioned challenges:

- Formulation of Ordinary Differential Equations (ODEs)-Net-enabled Dynamic Equivalence (NeuDyE): This approach leverages ODEs and neural networks to model the system dynamics accurately, providing a continuous-time, data-driven representation that aligns with the actual behavior of power grids.
- Introduction of Physics-Informed Neural Dynamic Equivalence (PI-NeuDyE): It combines an ODE-NET-enabled equivalent model with a physics-informed learning to identify a continuous-time dynamic equivalence while ensuring a close match in the closed-loop dynamic behaviors under disturbances.
- Implementation of a Driving Port NeuDyE (DP-NeuDyE): It reduces the number of inputs required for training, making it more manageable and cost-effective to deploy in real-world interconnected bulk power systems. Its generalization ability is also explored based on electrical distance.

This article is organized as follows: Section 2 introduces the mathematical basis of NeuDyE, i.e., how to formulate and simulate a power system with subsystems modeled by neural dynamic equivalence. Section 3 explains the key technology of PI-NeuDyE and DP-NeuDyE, i.e., using Neural-Ordinary-Differential-Equation-Network (ODE-NET) to discover the dynamic equivalence of power systems. Section 4 then introduces the procedure of the NeuDyE and presents extensive case studies on the 140-bus NPCC system [5]. The results demonstrate the effectiveness of NeuDyE and its capability to handle various contingencies. Section 5 states the conclusion.

## 2. PROBLEM FORMULATION

For a reliability coordinator (RC), the entire interconnection can be partitioned into an internal system (InSys) and the external systems (ExSys). A RC usually has both accurate dynamic models and real-time observability for InSys, but not ExSys. In reality, there may be a cushion area where the RC has partial observability; however, in this paper, we consider it part of the ExSys as well. Take the 140-bus NPCC system as an example, InSys and ExSys, connected through two tie lines [6], are illustrated in Figure 1.

InSys (bus1-36), which is the simplified ISO New England (ISO-NE) system, represents the subsystem that can be characterized by precise knowledge of its structure and parameters, enabling

straightforward formulation using dynamic models for each component. The model-based InSys can be formulated based on the known dynamics of each component (e.g., the generators, turbines, exciters, loads, converter controls, transmission lines) by a set of differential algebraic equations (DAE) in (2.1) (2.2).

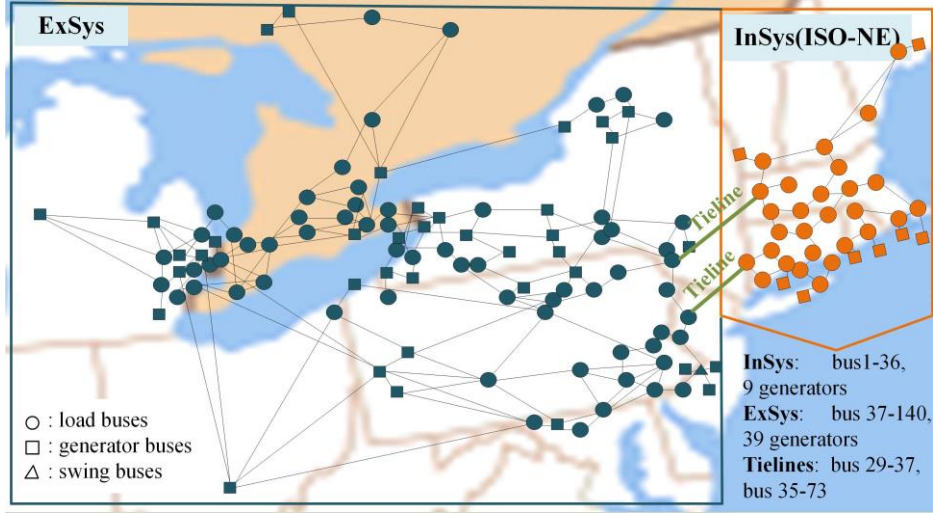


Figure 1 Topology of the NPCC system

In contrast, ExSys (bus37-140) lacks accessible physics models due to factors such as unavailable system state measurements, privacy concerns and inaccessible local measurements, e.g., real-time dispatch of the generators. Therefore, a data-driven neural network based dynamic equivalence is relied upon to model ExSys, as in (2.3) [7]:

$$\frac{dx_{in}}{dt} = \mathcal{P}(x_{in}, y_{in}, i_{tie}) \quad (2.1)$$

$$G(x_{in}, y_{in}, i_{tie}) = 0 \quad (2.2)$$

$$\frac{dx_{ex}}{dt} = \mathcal{N}(x_{ex}, z_{in}) \quad (2.3)$$

Here,  $x_{in}$  denotes the state variables of InSys's components (e.g., generators, turbines, exciters);  $y_{in}$  denotes the algebraic variables of InSys such as power flow states;  $i_{tie}$  denotes the currents flowing through the tie lines. Functions  $\mathcal{P}$  and  $G$  denote the dynamic and algebraic equations of InSys, respectively, which can be readily established based on the physics models of InSys.  $x_{ex}$  denotes the state variables of ExSys;  $z_{in}$  denotes the features from InSys, which is selected from part of the states of InSys to describe the interaction between InSys' dynamics and ExSys' dynamics.  $\mathcal{N}$  is the forward propagation function of a neural network, which mimics the ExSys dynamics. This neural network is multi-layer structured, whose forward propagation can be functionally expressed as:

$$\mathcal{N}(x_{ex}, z_{in}) = \mathcal{L}_m(\mathcal{L}_{m-1}(\cdots \mathcal{L}_1(x_{ex}, z_{in}, \theta_1) \cdots, \theta_{m-1}), \theta_m), \quad (2.4)$$

where  $\mathcal{L}_m$  denotes the loss function of the  $m^{th}$  layer and  $\theta_m$  denotes the corresponding weights in that layer. The universal approximation theorem ensures that a Deep Neural Network (DNN) can approximate any continuous functions for inputs within a specific range. Therefore, the advantage of a neural network-enabled dynamic equivalence lies in its flexibility for approximating a dynamic system without requiring the system to be linear or assuming any dynamical modes beforehand.

### 3. ODE-NET-ENABLED DYNAMIC EQUIVALANCE

#### 3.1 NECESSITY OF CONTINUOUS-TIME LEARNING

A neural network can be regarded as a nonlinear function characterized by parameters  $\theta$ . In machine learning, these parameters are optimized by minimizing a loss function, typically computed as the error between measurements and neural network outputs. However, in this problem, the difficulty lies in the fact that the output of the neural network is the derivative of  $x_{ex}$  while the measurements only provide  $x_{ex}$ , making the loss function hard to construct directly. To solve the problem, two different paths exist: discrete-time learning and continuous-time learning.

Conventional machine learning techniques for dynamic equivalence primarily rely on discrete-time learning. In discrete-time learning, the loss function for neural network training is usually constructed by discretizing the continuous-time differential equations into discrete-time difference equations. For example, based on the trapezoidal rule, the ExSys dynamics can be discretized as:

$$\frac{x_{ex}(t) - x_{ex}(t - \Delta)}{\Delta} = \frac{1}{2} (\mathcal{N}(x_{ex}(t), z_{in}(t)) + \mathcal{N}(x_{ex}(t - \Delta), z_{in}(t - \Delta))). \quad (3.1)$$

Correspondingly, the loss function can be established, and the neural network can be optimized by

$$\min_{\theta} \sum_{i=0}^n L_{discrete} = \sum_{i=0}^n \frac{1}{2} \eta_i \|y_i - \hat{y}_i\|_2, \quad (3.2)$$

where the subscript  $i$  denotes the time-step,  $n$  is the number of total time steps,  $\hat{y} = \frac{1}{\Delta} (\hat{x}_{ex}(t) - \hat{x}_{ex}(t - \Delta))$  denotes the derivatives estimated from the measurements; and  $y = \frac{1}{2} (\mathcal{N}(x_{ex}(t), z_{in}(t)) + \mathcal{N}(x_{ex}(t - \Delta), z_{in}(t - \Delta)))$  denotes the derivatives estimated from the neural network;  $\eta_i$  denotes the weighting factor at time step  $i$ .

However, this approach is sensitive to derivative estimation, resulting in biased training outcomes due to residue errors during training or non-ideal measurements. Although discrete-time training may produce satisfactory derivatives fitting, it cannot guarantee the accuracy of system states after numerical integration, leading to unsatisfactory performance in learning continuous-time dynamics.

Our solution is an ODE-NET-enabled dynamic equivalence, which adopts a continuous-time learning philosophy by directly minimizing the error between the state measurements  $\hat{x}$  and the numerical solution of (2.4):

$$\begin{aligned} \min_{\theta} \sum_{i=0}^n L(x_{ex,i}) &= \sum_{i=0}^n \frac{1}{2} \eta_i \|x_{ex,i} - \hat{x}_{ex,i}\|_2 \\ \text{s.t. } \frac{dx_{ex,i}}{dt} &= \mathcal{N}(x_{ex}, \hat{z}_{in}, \theta) \end{aligned} \quad (3.3)$$

Comparing (3.2) with (3.3), an obvious distinction is that ODE-NET is capable of directly minimizing the difference between real dynamic states and trained dynamic states, which requires no discretization and fully respects the continuous-time characteristics of power system dynamics. Therefore, it is theoretically less vulnerable to non-ideal measurements and the residue training error.

### 3.2 PHYSICS-INFORMED CONTINUOUS-BACKPROPAGATION

Traditional DNNs are generally trained by the backpropagation technique, which computes the gradient of the loss function with respect to the DNN parameters at each layer to update the DNN. However, the ODE-NET training shown in (3.3) differentiates from the conventional loss function (such as (3.2)) because it involves the numerical integration in its constraints. To deal with the integration-incorporated constraints, ODE-NET adopts a continuous backpropagation technique to perform the neural network training. An adjoint method [7][8] is introduced to transform (3.3) into a

format that removes the numerical integration constraints; then a physic-informed (PI) continuous-backpropagation technique is developed as follows:

$$\begin{aligned}
\min_{\theta} \sum_{i=0}^n L(x_{ex,i}, x_{in,i}) &= \sum_{i=0}^n \frac{\eta_i}{2} (\|x_{ex,i} - x_{ex,i}\|_2 + \|x_{in,i} - x_{in,i}\|_2) \\
\mathcal{L} &= \sum_{i=0}^n L_i - \int_{t_0}^{t_n} \left[ \lambda^T (\dot{x}_{ex} - \mathcal{N}_{\theta}) + \mu^T (\dot{x}_{in} - \tilde{\mathcal{P}}) \right] dt \\
s.t. \quad x_{ex,i} &= x_{ex,0} + \int_{t_0}^{t_i} \mathcal{N}(x_{ex}, z_{in}, \theta) dt \\
x_{in,i} &= x_{in,0} + \int_{t_0}^{t_i} \mathcal{P}(x_{in}, y_{in}, i_{tie}) dt
\end{aligned} \tag{3.4}$$

where  $\lambda$  and  $\mu$  respectively denote the adjoint states for ExSys and InSys,  $\tilde{\mathcal{P}}$  is equivalently formulated from  $\mathcal{P}$  using (2.2). A dynamic equivalence is theoretically non-autonomous, where the InSys' states also impact the ExSys' dynamics. Thus, the dynamics of InSys and ExSys are both considered in (3.4), which assures the performance of ODE-NET in the closed-loop simulation of the whole power system. With proper adjoint boundary conditions [8], the physics-informed gradient is:

$$\begin{aligned}
\frac{d}{dt} \begin{bmatrix} \lambda^T \\ \mu^T \\ \partial \mathcal{L} / \partial \theta \end{bmatrix} &= \begin{bmatrix} -\lambda^T \partial \mathcal{N} / \partial x_{ex} - \mu^T \partial \tilde{\mathcal{P}} / \partial x_{ex} \\ -\lambda^T \partial \mathcal{N} / \partial x_{in} - \mu^T \partial \tilde{\mathcal{P}} / \partial x_{in} \\ \lambda^T \partial \mathcal{N} / \partial \theta \end{bmatrix} \\
\theta &\leftarrow \theta - \frac{\partial \mathcal{L}}{\partial \theta}
\end{aligned} \tag{3.5}$$

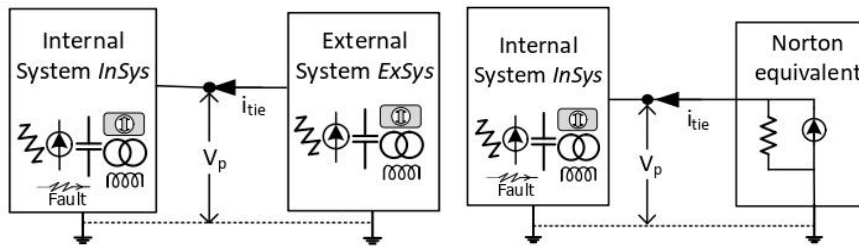
Finally, the gradient descent for  $\mathcal{N}_{\theta}$  can be performed using  $\partial \mathcal{L} / \partial \theta|_{t=0}$  integrated from (3.5) by any ODE solvers.

### 3.3 NETWORK EQUIVALENT SEEN FROM DRIVING PORT

In the previously devised PI-NeuDyE, the optimal closed-loop results are achieved using extensive inputs from the internal system, which may not be readily available in practical applications. To make the method applicable in such scenarios, we develop an enhanced neural equivalent technique called the Driving Port (DP) NeuDyE which only needs the knowledge of boundary voltages  $v_p$  for the tie-lines, empowering the practical implementations of NeuDyE in utilities and ISOs.

#### 3.3.1 Algebraic component separation

To form the neural network-integrated power grid, following equations (2.1)-(2.3), the selection of  $x_{ex}$  and  $z_{in}$  is necessary. If ExSys is static, a Norton equivalent current source, depicted in Figure 2(b), can replace it. From the perspective of InSys, the representation of ExSys in full detail or as a Norton equivalent current source yields the same output  $i_{tie}$  for the given input  $v_p$ .



(a) Original networks (b) Norton equivalent  
Figure 2 Network equivalent methodologies

Inspired by the Norton equivalent theory, we develop a neural network observed from the driving port. To capture its nonlinear dynamics, measurements of port voltages  $v_p$  and tie currents  $i_{tie}$  are utilized to discover the state space model of ExSys as shown in Figure 2(b). The tie currents  $i_{tie}$  are selected as the state variables for external system  $x_{ex}$ , whose continuous differential structure is represented by the neural network; then a magic touch, the algebraic component separation, is introduced below:

$$\begin{aligned}\frac{di_{tie}}{dt} &= \mathcal{N}(i_{tie}, v_p, \theta) \\ \mathcal{G}(i_{tie}, v_p) &= 0\end{aligned}\quad (3.6)$$

where the port voltages  $v_p$  corresponds to the InSys features  $z_{in}$  in (2.3). The tie currents  $i_{tie}$  can then be represented as a linear combination of state variables and inputs, i.e.:

$$i_{tie} = C_s \cdot x_{ex} + D \cdot v_p \quad (3.7)$$

where matrices  $C_s$  and  $D$  are constant matrices. If a fault happens in the internal network at time instant  $t_i$ , sudden changes may happen in  $\Delta v_p(t_i) = v_p(t_i + \Delta t) - v_p(t_i)$ , while  $x_{ex}(t_i)$  keeps invariant in a very short period of  $\Delta t$ , i.e.  $\Delta x_{ex}(t_i) = 0$ .

The components  $i_{tie}$  can be split into two types of components: continuous-state-variable components  $i_{tie\_cs} = C_s \cdot x_{ex}$  and algebraic components  $i_{tie\_a} = D \cdot v_p$ . Algebraic components embody the immediate contribution from the port voltages  $v_p$ , which may exhibit discontinuity during switching events within the internal network. On the other hand, continuous-state-variable components,  $i_{tie\_cs}$ , are employed as the constituents of the neural network equivalent, as illustrated in equation (3.6). These components fulfill the need for continuity as depicted in equation (3.6).

To compute the coefficient matrix  $D$ , we leverage measurement data obtained during the fault period. This is achieved by using the least squares method, as shown below:

$$\begin{bmatrix} D_{11} & \cdots & D_{1n_p} \\ \vdots & \ddots & \vdots \\ D_{n_p 1} & \cdots & D_{n_p n_p} \end{bmatrix} = \begin{bmatrix} \Delta i_{tie}(t_1) & \cdots & \Delta i_{tie}(t_{n_f}) \end{bmatrix} \cdot \begin{bmatrix} \Delta v_p(t_1) & \cdots & \Delta v_p(t_{n_f}) \end{bmatrix}^{-1} \quad (3.8)$$

where  $n_p$  is the number of port voltages and  $n_f$  is the number of faults whose port voltages and tie line currents are recorded in the data sets. Define  $\Delta v_p(t_i) = v_p(t_i + \Delta t) - v_p(t_i)$  and  $\Delta i_{tie}(t_i) = i_{tie}(t_i + \Delta t) - i_{tie}(t_i)$ . The continuous component  $i_{tie\_cs}$  can then be extracted as:

$$i_{tie\_cs} = i_{tie} - D \cdot v_p \quad (3.9)$$

The neural equivalent network in (3.6) and the DAE now become:

$$\begin{aligned}\frac{di_{tie\_cs}}{dt} &= \mathcal{N}(i_{tie\_cs}, v_p, \theta) \\ \frac{dx_{in}}{dt} &= \mathcal{P}(x_{in}, y_{in}, i_{tie}) \\ \mathcal{G}(x_{in}, y_{in}, i_{tie\_cs}, i_{tie}, v_p) &= 0\end{aligned}\quad (3.10)$$

The neural equivalent of the external system and the corresponding formulated interface as shown in Figure 3 are integrated into Transient Stability Analysis (TSA) simulation. The equivalent

admittance is formed by the coefficient matrix  $D$  (admittance matrix) in (3.9). The values of current sources are updated by applying an explicit integration method to (3.10).

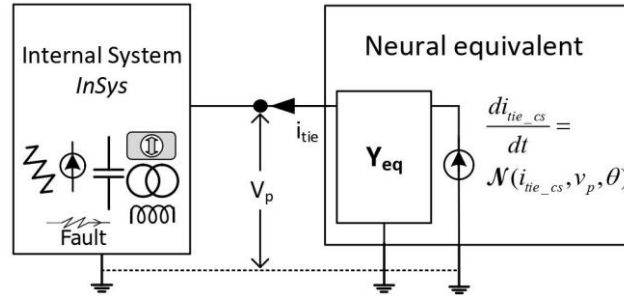


Figure 3 TSA interface for neural network equivalent

### 3.3.2 Formulation of ODE-NET Based State-Space Model

In real-world power networks, measurement data is inherently discrete, even though the underlying system is continuous. In the absence of assumptions regarding the dynamic model types, ODE-NET directly discovers the continuous-time dynamic model, as depicted in (3.10), from discrete measurements  $i_{tie}$  and  $v_p$ . During the time interval from  $0 \sim t_n$ , ODE-NET is trained by minimizing the loss function defined by the error between the state measurements  $\hat{i}_{tie\_cs}$  and the numerical solution  $i_{tie\_cs}$  by (3.10), as illustrated below:

$$L = \sum_{i=0}^n \frac{1}{2} \| i_{tie\_cs}(t_i) - \hat{i}_{tie\_cs}(t_i) \|_2 \quad (3.11)$$

where  $i_{tie\_cs}(t_i) = \hat{i}_{tie\_cs}(0) + \int_0^{t_i} \mathcal{N}(x, u, \theta) dt$ .

Similar as in (3.5), the challenge in minimizing (3.11) stems from the integration operation in the constraints. ODE-NET tackles this challenge by treating the ODE solver (the integration operation) as a black box and computing gradients using the adjoint sensitivity method [9][10], as depicted below with  $a = \partial L / \partial i_{tie\_cs}$ :

$$\frac{d}{dt} \begin{bmatrix} a^T \\ \partial L / \partial \theta \end{bmatrix} = \begin{bmatrix} -a^T \cdot \frac{\partial \mathcal{N}}{\partial i_{tie\_cs}} \\ a^T \cdot \frac{\partial \mathcal{N}}{\partial \theta} \end{bmatrix} \quad (3.12)$$

### 3.3.3 Strengthening ODE-NET Based on Recurrent Neural Network

Data-driven methodologies predominantly depend on observable states to construct the neural equivalent model, as exemplified in equation (3.6). However, this model reduction approach inherently leads to a scenario where state variables constitute only a minor subset of the comprehensive state variables present in the original power network. As a result, such a reduction may not entirely encapsulate all the crucial dynamic properties intrinsic to the power system.

To address this deficiency of information, we enhance the DP-NeuDyE in this section by leveraging historical data through the implementation of Recurrent Neural Networks (RNNs). RNNs, with their unique ability to remember past information, provide a robust mechanism to incorporate temporal dynamic behavior into the model. This allows for a more comprehensive understanding of the system dynamics, thereby improving the model's performance. The integration of RNNs into the DP-NeuDyE framework is illustrated in Figure 4 and explained as follows.

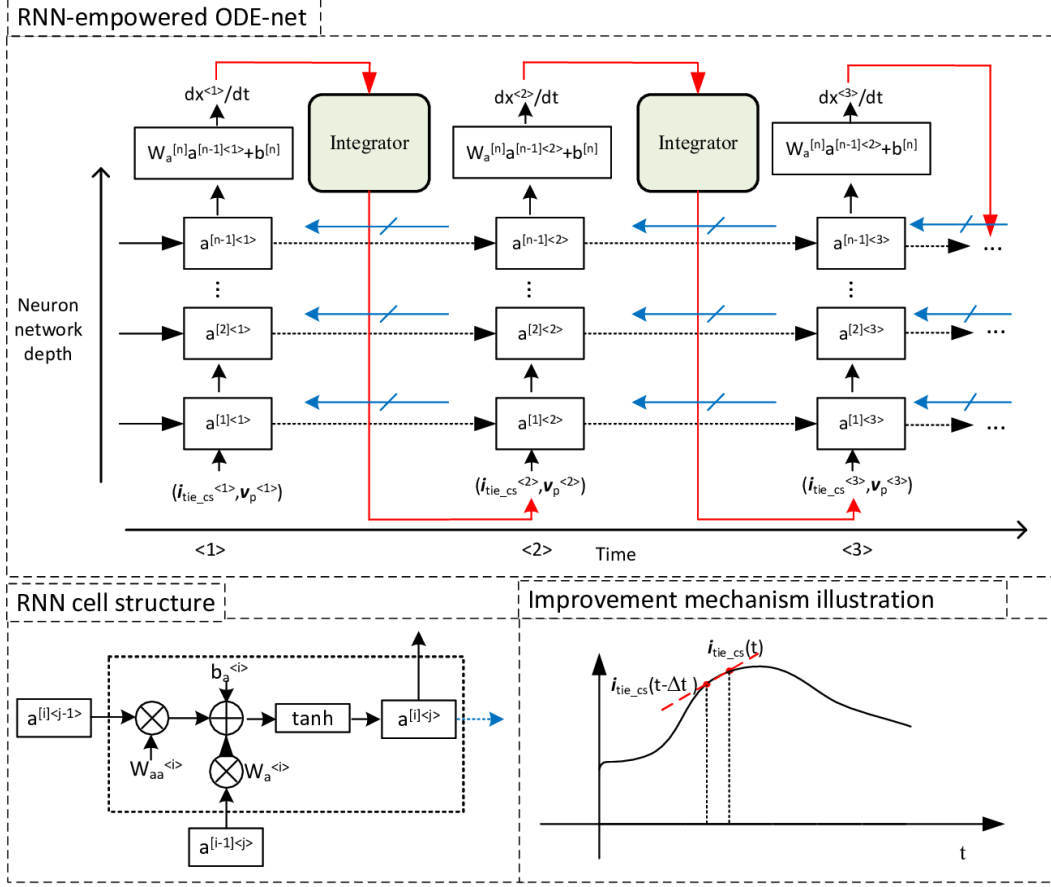


Figure 4 RNN empowered ODE-NET

The differential term  $di_{tie\_cs}/dt$  can be represented as:

$$\frac{di_{tie\_cs}}{dt} = \lim_{\delta \rightarrow 0} \frac{i_{tie\_cs}(t) - i_{tie\_cs}(t - \delta)}{\delta} \approx \frac{i_{tie\_cs}(t) - i_{tie\_cs}(t - \Delta t)}{\Delta t} \quad (3.13)$$

where  $\Delta t$  denotes a short period of time. Equation (3.13) implies that the historical information at time instant  $t - \Delta t$  could help determine the derivative at time instant  $t$ . Therefore, we devise a strategy to strengthen ODE-NET based on recurrent neural network (RNN) [11]. As illustrated in Figure 4, the structure of the Recurrent Neural Network (RNN) cell integrates the output of a specific neuron from the previous time step into the computation of the current time step's output for the same neuron. This mechanism effectively leverages historical data from the preceding time step to assist in calculating the derivative of the current time step. Therefore, this approach ameliorates potential information deficiencies that might arise when computations rely on a limited subset of state variable, thereby bolstering the overall accuracy and robustness of DP-NeuDyE.

Similar as in 3.3.2, the backward propagation should be used to evaluate the gradient of the neural network parameters. Recall that the continuous backpropagation for ODE-NET in 3.3.2 already considers integration along the time by solving an augmented differential equation. Therefore, the backward propagation throughout time for the RNN cell is ignored and the gradient descent method used in 3.3.2 can directly be applied to the RNN-empowered ODE-NET.

#### 4. CASE STUDY

In this section, the detailed training and testing procedures of NeuDyE are introduced. Simulation results of PI-NeuDyE and DP-NeuDyE are presented to demonstrate their efficacy and practicality.

## 4.1 TRAINING DETAIL

The ground truth electromechanical trajectories are obtained by simulating the complete, physics-based 140-bus NPCC system via the Power System Toolbox (PST) [12]. The PST results are verified with simulations from Transient Security Assessment Tool (TSAT). Trapezoidal rule is adopted as the numerical integration method for the devised method.

### 4.1.1 Open-loop, data-driven ODE-NET Training

PI-ODE-NET: as introduced in Subsection 3.2.2, the selected states are from generators, exciters, governors, and line currents of InSys as  $s_{in}$ , in total 90 dimensions; the tie line currents are the states of ExSys  $x_{ex}$  with 4 dimensions (2 tie lines, each has a real part and an imaginary part). Note that such training features can be flexibly adjusted according to available measurements. If the training features are abundant, the training process might be slower because of the numerical integration burden.

RNN-empowered DP-ODE-NET: followed by 3.3,  $s_{in}$  includes boundary voltages with 4 dimensions (2 ports, each with a real part and an imaginary part);  $x_{ex}$  consists of tie line currents; as such, DP-ODE-NET is faster than PI-ODE-NET. However, this comes at the expense of compromising the model's generalization ability, resulting in less accurate predictions for unseen scenarios.

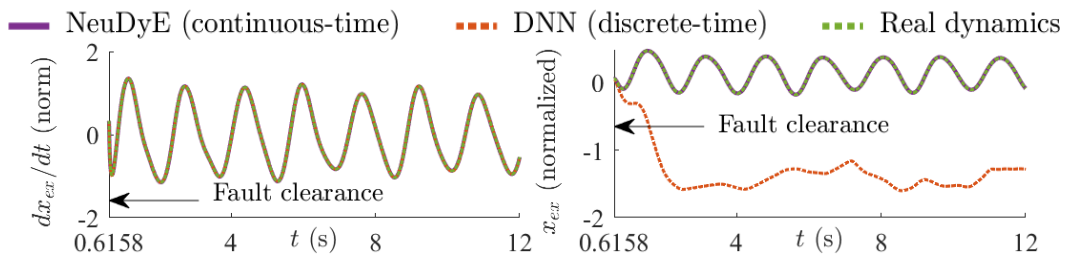
### 4.1.2 Closed-Loop Testing

After an ODE-NET is obtained, the closed-loop tests check its performance. Closed-loop means the ODE-NET-based ExSys model replaces the large-unknown external systems and integrates with the physics-based InSys model. This is the final setup. The entire system's dynamics are then computed through numerical integration. The predicted values are trajectories simulated by the physics-neural-integrated system, which contains the 36-bus, physics-based InSys and the ODE-NET-based dynamic equivalence of the ExSys. If the NeuDyE can accurately mimic the dynamics of the original ExSys, the predicted values should be close to the true values, i.e., simulation with the full system model.

## 4.2 SIMULATION RESULTS

### 4.2.1 Varied fault clearing times and fault locations using PI-NeuDyE

As mentioned in 3.1, traditional discrete learning may yield satisfactory predictions in open-loop training by fitting the derivatives, like in Figure 5(a), which is the prediction from a deep neural network (DNN). Whereas in the closed-loop test in Figure 5(b), DNN fails to capture the continuous dynamics after the integration, showing the necessity of the continuous-time learning.



(a) Open-loop training performance (b) Closed-loop testing performance

Figure 5 Comparison of NeuDyE with conventional discrete-time DNN

Depicted in Figure 6 and Figure 7, 25 training scenarios are generated by launching three-phase faults at 0.50s at bus 18, 19, 20, 21, or 28 with fault clearing set randomly within a time interval [0.53s, 0.6s]. The training variables of InSys have 90 dimensions as mentioned in 4.1.1. Figure 6 shows the schematic diagram of PI-NeuDyE and the test results on bus 21 with faults cleared at 0.54s, 0.56s, and 0.58s, which are new values to the training sets. Trajectories of boundary voltage of bus 35 demonstrate a perfect match between PI-NeuDyE's results and that from the full NPCC model.

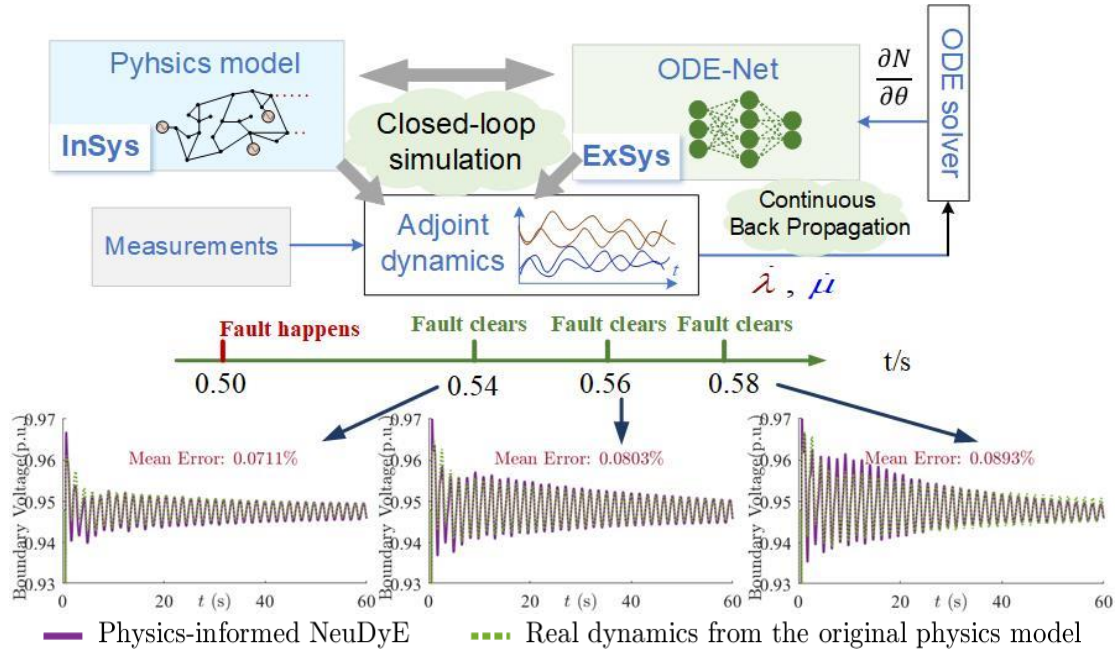


Figure 6 Closed-loop test results of fault on bus 21 with different clearing times

Figure 7 shows the test results at different buses with faults all cleared at 0.54s, showing that PI-NeuDyE is also effective in handling changes in fault locations. Figures 6 and 7 together show that the derived PI-NeuDyE model can properly and accurately represent the dynamics and transients, regardless of changes in fault durations or fault locations.

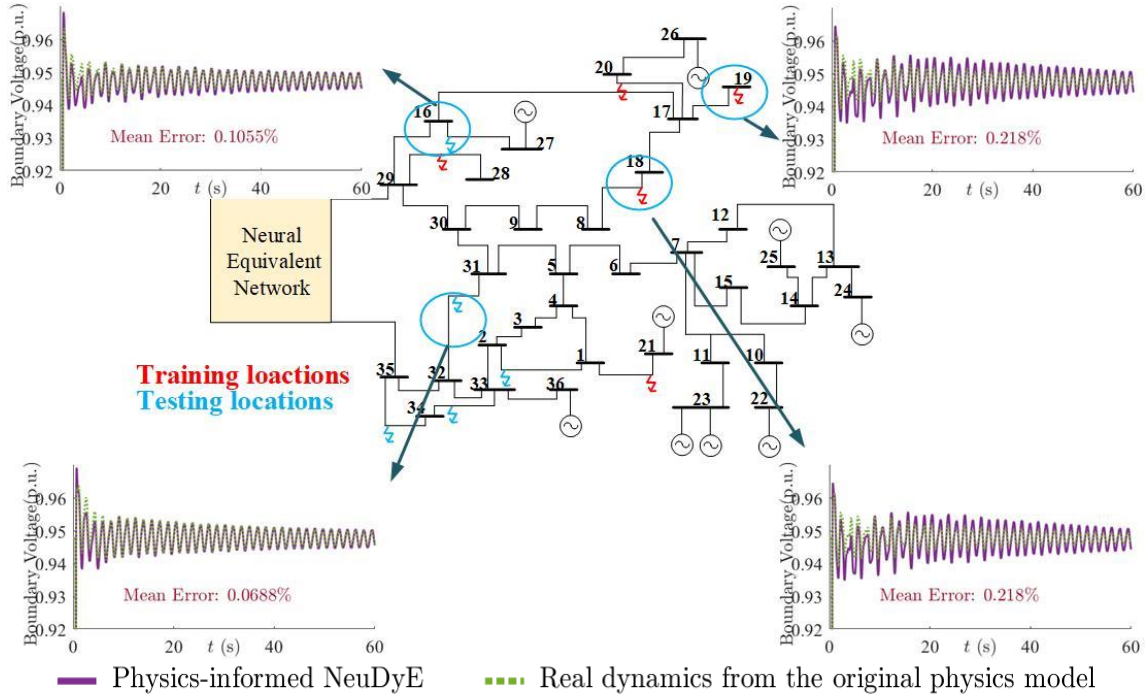


Figure 7 Closed-loop test results of fault with different locations

Further, in Figure 8, 108 testing scenarios are generated with new fault locations and random fault clearing times at bus 2, 5, 9, 16, 25, 28, 32, 34 and 35. The box plot shows that the overall relative error is lower than 1%, indicating a satisfying generalization ability.

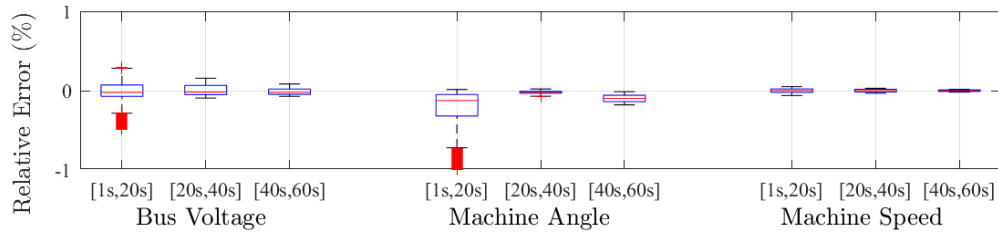


Figure 8 Accuracy of PI-NeuDyE under 108 cases with new fault locations and random clearing times

As mentioned in 4.1.1, choosing features of InSys is flexible. Other settings, like using active and reactive power of transmission lines or bus voltages and line currents, are also feasible. As an example, Figure 9 presents a new testing result by using boundary voltages between ExSys and InSys and all branch currents in InSys as training features (90 dimensions for InSys). The predicted trajectories match with the measurements closely, with a mean error of less than 0.3%, indicating high accuracy and satisfactory performance of NeuDyE using different settings of training features.

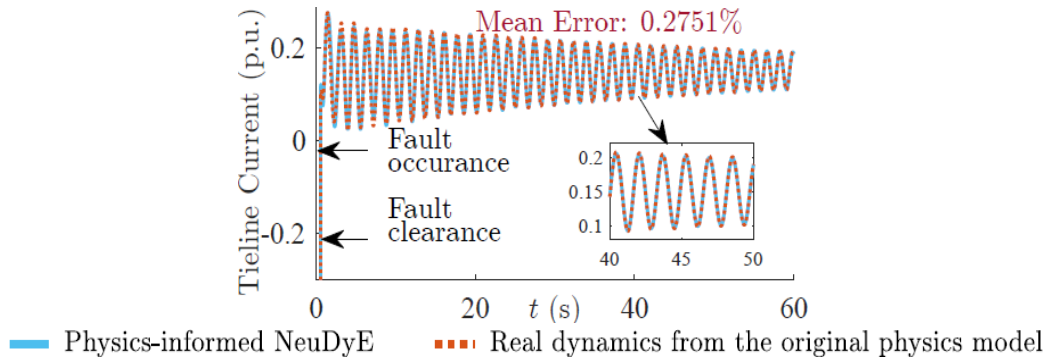


Figure 9 PI-NeuDyE closed-loop results using all branch currents and boundary voltages in InSys.

#### 4.2.2 Reduced variables using DP-ODE-NET

As previously mentioned, DP-NeuDyE is designed for potential practical applications that requires limiting the number of input variables. In contrast with 4.2.1, where the number of InSys features used in Figure 9 and Figures 6-8 are 90 dimensions, DP-NeuDyE only needs 4 dimensions of InSys features. The selections of ExSys features are the same for both methods. The ExSys subsystem, as depicted in Figure 1, is modeled by the DP-ODE-NET as illustrated in Figure 10.

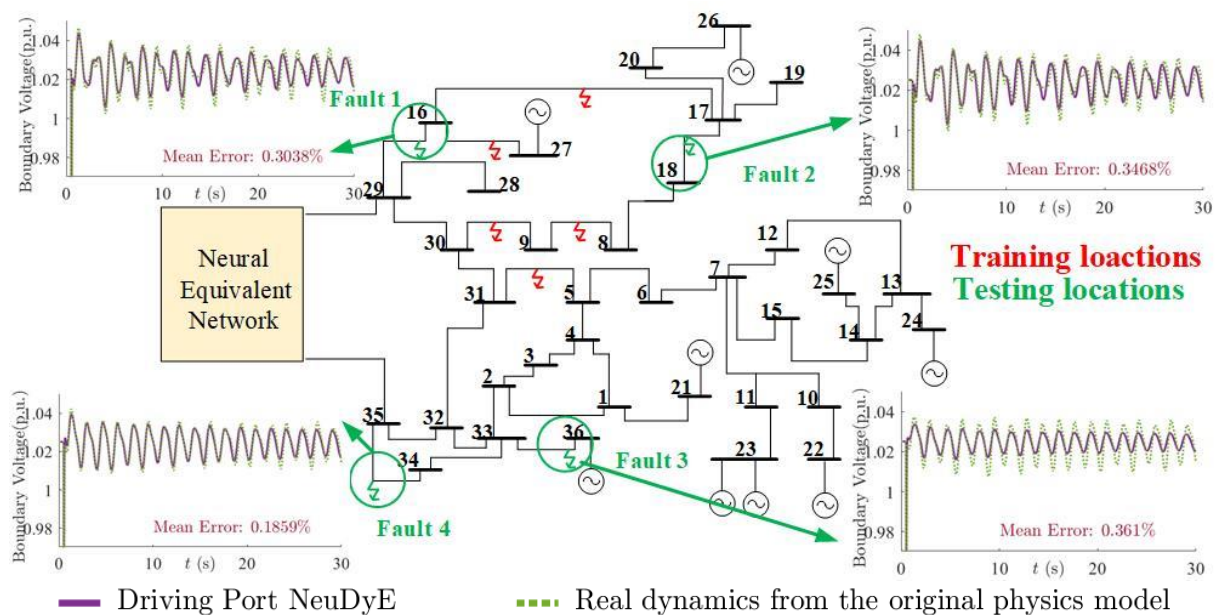


Figure 10 DP-NeuDyE closed-loop simulation.

This model is derived from five distinct dynamic trajectories, each triggered by phase-to-ground faults at the T-line, as highlighted in red in Figure 10. Using the derived model, we generated the low-frequency oscillation trajectories. Each oscillation is initiated by a phase-to-ground fault at the T-line within the green circle. The green arrows represent faults that have not been encountered in the training set (historical record).

The trajectories generated by the full detailed model simulation are also drawn as dotted lines in Figure 10. It can be observed that DP-NeuDyE is able to precisely predict the low frequency oscillations in a fairly large area. Since this scenario is not in the training set, the predictability of the proposed method is validated. Besides, there are two oscillation modes in the full model-based trajectory: 0.5991 Hz with a magnitude of 0.2155 and 1.24813 Hz with a magnitude of 0.1349. The neural equivalent model-based simulation also accurately predicts those oscillation modes, with a magnitude of 0.2051 and 0.1431 respectively.

### 4.2.3 Generalizability analysis based on electrical distance

To quantify the NeuDyE models' generalization performance, we employ the electrical distance between the fault locations in the testing set and those in the training set as a measure. The network topology is transformed into an adjacency matrix using graph theory, as depicted in equation (4.1), thereby establishing an automated method for predicting the performance of the introduced neural ODE model for subsystems. Consequently, the electrical distance between a new fault location and those in the training set can be determined from the adjacency matrix by selecting the shortest distance.

$$\text{Adjacency matrix } A: \begin{cases} \text{Electric connection between BUS } i \text{ and } j: A_{ij} = X_{ij} \\ \text{Else: } A_{ij} = 0 \\ \text{Fault dynamic record near BUS } i: A_{ii} = 1 \end{cases} \quad (4.1)$$

where  $i \neq j$  and  $X_{ij}$  is the reactance (p.u.) in the branch connecting *BUS*  $i$  and  $j$ .

In the previous case study as depicted in Figure 10, the electrical distances from the test set to the training set are as follows: 0, 0.0255, 0.0404, 0.0369. These electrical distances are relatively small; the generalizability of the DP-NeuDyE is thus relatively good. However, if a fault occurs at a considerably remote distance from those in the training set, such as the T-line between bus 19 to 17, where the electrical distance is 0.0948, the neural equivalent model may encounter challenges in making accurate dynamic predictions, as illustrated in Figure 11(a).

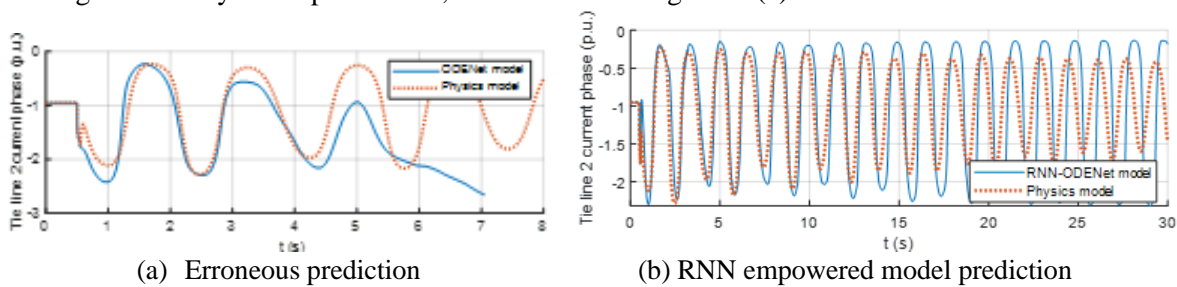


Figure 11 RNN-empowered DP-ODE-NET simulation

That is exactly when RNN-empowered ODE-NET shows its advantage of a better generalization ability. For the same training set and testing scenario, the trajectory by the RNN-empowered neural equivalent model is shown in Figure 11(b). Instead of giving a diverged result, RNN-empowered ODE-NET provides a satisfying prediction, especially for the time period after the fault.

Despite the convergence achieved by RNN-empowered DP-NeuDyE from this distant fault location, its performance is still not as commendable as PI-NeuDyE shown in Figure 7, top right subfigure. The primary reason behind this discrepancy lies in the training process. PI-NeuDyE trains in a closed-loop manner by considering the interacting dynamics of both InSys and ExSys, involving 90 dimensions of

InSys features. Whereas DP-NeuDyE only sees from the driving port, utilizing only 4 dimensions of boundary measurements as InSys features. As a result, there exists a trade-off between training efficiency and generalization ability, which impacts the overall performance of the DP-NeuDyE. For fault not too distant from the training sets, both DP-NeuDyE and PI-NeuDyE yield satisfactory results.

## 5. CONCLUSION

This article introduces a physics-integrated Neural Dynamic Equivalence (PI-NeuDyE) and its practical application Driving Port NeuDyE (DP-NeuDyE), which uncovers a powerful continuous-time dynamic equivalence of external systems. One of its key advantages is the ability to preserve the continuous-time dynamic characteristics of power grids while using fewer variables. The effectiveness of DP-NeuDyE and PI-NeuDyE are demonstrated through case studies conducted on the 140-bus NPCC system, showcasing their performance under various fault locations and clearing times. Furthermore, comparisons are made between DP-NeuDyE and PI-NeuDyE in terms of efficiency and generalization ability.

## BIBLIOGRAPHY

- [1] M. L. Ourari, L.A. Dessaint, and V.-Q. Do, "Dynamic equivalent modeling of large power systems using structure preservation technique," *IEEE Transactions on Power Systems*, vol. 21, no. 3, pp. 1284–1295, 2006.
- [2] Y. G. I. Acle, F. D. Freitas, N. Martins, and J. Rommes, "Parameter preserving model order reduction of large sparse small-signal electromechanical stability power system models," *IEEE Transactions on Power Systems*, vol. 34, no. 4, pp. 2814–2824, 2019.
- [3] I. Tyuryukanov, M. Popov, M. van der Meijden, and V. Terzija, "Slow coherency identification and power system dynamic model reduction by using orthogonal structure of electromechanical eigenvectors," *IEEE Transactions on Power Systems*, vol. 36, no. 2, pp. 1482–1492, 2020.
- [4] N. Tong, Z. Jiang, S. You, L. Zhu, X. Deng, Y. Xue, and Y. Liu, "Dynamic equivalence of large-scale power systems based on boundary measurements," in *2020 American Control Conference (ACC)*, pp. 3164–3169, IEEE, 2020.
- [5] Y. Lei, Y. Liu, G. Kou, B. Wang, "A study on wind frequency control under high wind penetration on an NPCC system model," *2014 IEEE PES General Meeting, Conference & Exposition, National Harbor, MD, USA, 2014*, pp. 1-5.
- [6] Dylewsky, Daniel & Yang, Xiu & Tartakovsky, Alexandre & Kutz, J. (2019). Engineering structural robustness in power grid networks susceptible to community desynchronization. *Applied Network Science*. 4. 10.1007/s41109-019-0137-0.
- [7] Q. Shen and Y. Zhou, "Physics-Aware Neural Dynamic Equivalence of Power Systems," *IEEE Transactions on Power Systems*, under review.
- [8] Y. Zhou and P. Zhang, "Neuro-reachability of networked microgrids," *IEEE Transactions on Power Systems*, vol. 37, no. 1, pp. 142–152, 2022.
- [9] R. T. Q. Chen, Y. Rubanova, J. Bettencourt, and D. K. Duvenaud, "Neural ordinary differential equations," vol. 31, 2018.
- [10] L. S. Pontryagin, "Mathematical theory of optimal processes", CRC press, 1987.
- [11] D. E. Rumelhart, G. E. Hinton, and R. J. Williams, "Learning representations by back-propagating errors," *nature*, vol. 323, no. 6088, pp. 533–536, 1986. 19.
- [12] J. H. Chow, *Power System Toolbox (PST)*.